

# Activation Template Matching Loss for Explainable Face Recognition

Huawei Lin      Haozhe Liu      Qiufu Li      Linlin Shen\*

Computer Vision Institute, Shenzhen University, Shenzhen 518060, China  
 Shenzhen Institute of Artificial Intelligence and Robotics for Society, Shenzhen 518060, China  
 Guangdong Key Laboratory of Intelligent Information Processing, Shenzhen University, Shenzhen 518060, China

huaweilin.cs@gmail.com      liuhaozhe2019@email.szu.edu.cn  
 {liqiufu, llshen}@szu.edu.cn

## Abstract

Can we construct an explainable face recognition network able to learn a facial part-based feature like eyes, nose, mouth and so forth, without any manual annotation or additional datasets? In this paper, we propose a generic Explainable Channel Loss (ECLoss) to construct an explainable face recognition network. The explainable network trained with ECLoss can easily learn the facial part-based representation on the target convolutional layer, where an individual channel can detect a certain face part. Our experiments on dozens of datasets show that ECLoss achieves superior explainability metrics, and at the same time improves the performance of face verification without face alignment. In addition, our visualization results also illustrate the effectiveness of the proposed ECLoss.

## 1. Introduction

Face recognition has made significant achievement in the past ten years [42, 50, 14, 25, 24, 63], due to the development of deep learning, large-scale labeled faces datasets and so forth, and has been extensively used in many applications [23, 61]. Despite of the great success, most of these face recognition algorithms are still "black-box".

What face recognition networks have learned? It is commonly believed that the shallow layers are more likely to capture low-level information like colors, edges, and textures, while deep layers tend to describe high-level features [66, 29]. However, such observation is too general to understand a face recognition network.

A typical approach of previous studies for this problem is to use saliency map to understand a network when it makes a decision [2, 76, 19, 51, 33]. However, most saliency map based methods are not suitable for face recognition, as the areas of maximum activation are focused on the whole face

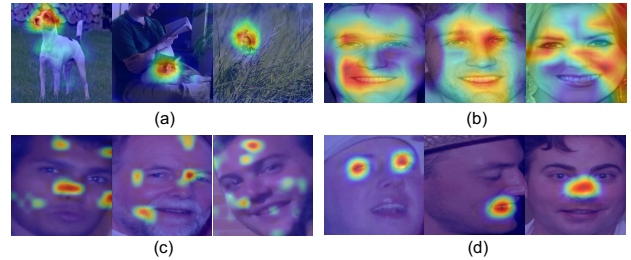


Figure 1. Comparison between different methods. (a) In object classification, the visualization of Grad-CAM[51] shows reasonable network prediction. The maximum activation regions (red) tend to cover the actual objects. (b) In face recognition, The maximum activation regions visualized by Grad-CAM[51] focus on the whole face mostly, and does not provide effective evidence for explainability. (c) Feature map visualization for face recognition. The pattern of activation is random, and can not be understood by humans. (d) Feature map visualization for our explainable face recognition. A channel of feature maps represents a certain face part.

as shown in Figure 1, which does not provide effective evidence and semantic information for explainability. Prior works have demonstrated that the representation extracted by deep networks may be mixed with high-dimensional abstract features that humans cannot understand.

One potential solution for this issue is to guide the networks to learn a structural representation [64]. Yin *et al.* [64] suggested that in explainable face recognition network, each channel shall be able to represent a face part, and proposed a spatial activation diversity loss to learn an explainable representation. However, in order to learn explainable representation patterns, occluded faces are required for training. This additional step undoubtedly increases the difficulty of training. How can we find out a model-agnostic method to construct an explainable face recognition network without any additional occlusion face dataset?

Inspired by previous studies on the explainability and

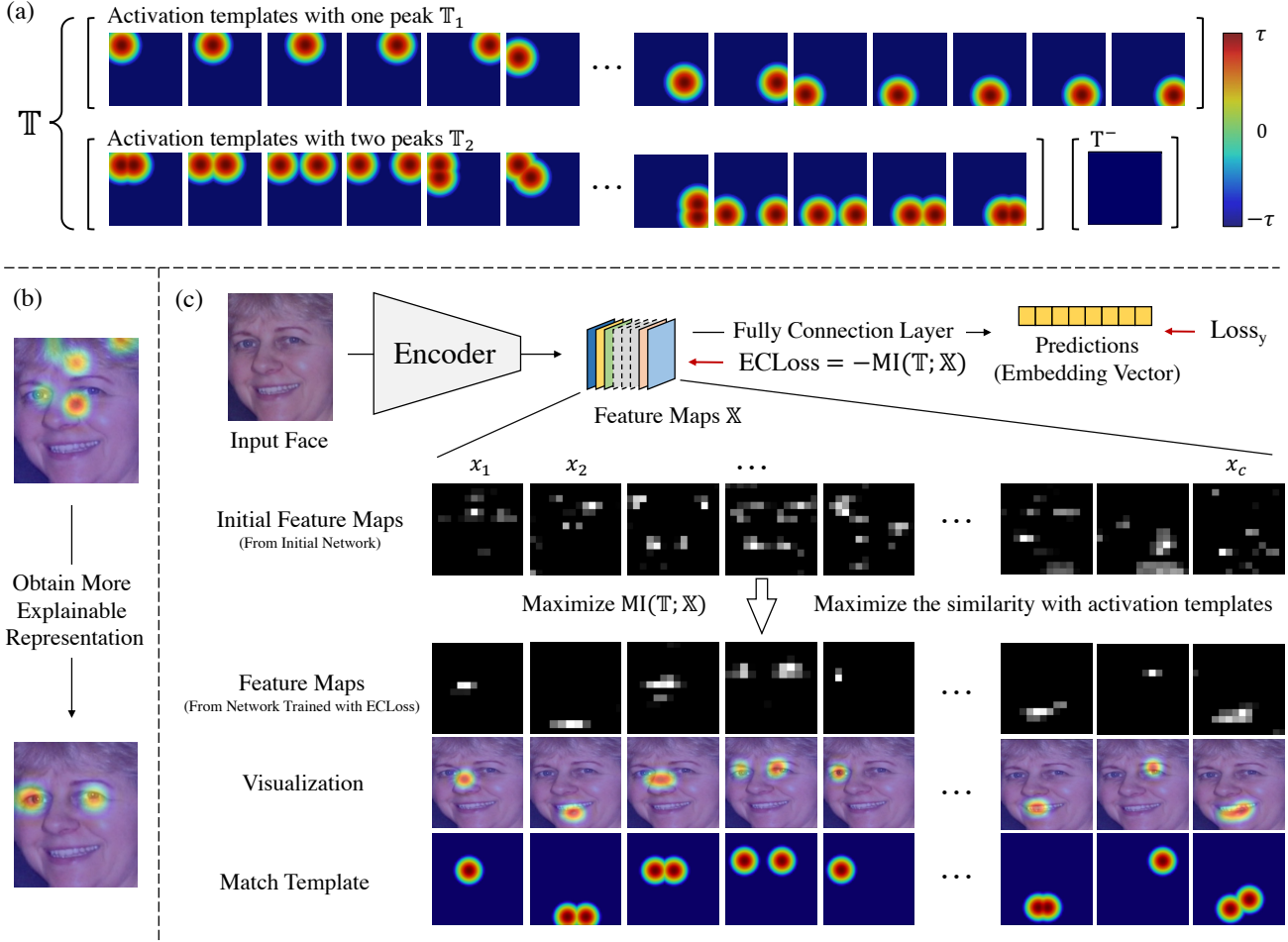


Figure 2. The training pipeline of explainable network with the proposed ECLoss. (a) The activation templates  $\mathbb{T}$  are used for ECLoss to force the representations of the target convolutional layer to contain maximum two activation peaks. (b) Compared with the network trained without ECLoss, the explainable network trained with ECLoss can obtain more explainable representation on the target convolutional layer. (c) The pipeline of training. The proposed ECLoss used mutual information, to force the target convolutional layer to represent the patterns of the activation templates.

interpretability of deep learning [68, 64, 3, 76, 3, 75, 4, 32], we proposed a generic Explainable Channel Loss (ECLoss) to construct an explainable face recognition network. Figure 1 shows the difference in feature maps among different methods. By adopting ECLoss, the recognition network can stand a more readable representation for its decision behavior, which draw a remarkable progress over the existing explainable solutions. As shown in Figure 2, a channel of the explainable face recognition network trained with ECLoss can learn semantic parts like eyes, mouth, nose, etc. To the best of our knowledge, this is the first method to construct a feature level explainable face recognition network that does not require any additional dataset or manual annotation. In this way, the explainable network is able to effectively demonstrate what has been learned.

In conclusion, the proposed Explainable Channel Loss

(ECLoss) has the following properties:

- 1) Networks trained with ECLoss can explain what is learned inside the network. As shown in Figure 6, the visualization results show that different channels learned different semantic parts.
- 2) As shown in Figure 2 and Figure 6, a single channel within the explainable face recognition network trained with ECLoss can learn different semantic parts like eyes, mouth, nose, etc.
- 3) Compared to [68], the training of ECLoss in the network is simple and effective, and does not require any manual annotation. *i.e.* labeling of nose, mouth, or other parts are not necessary.
- 4) As a model-agnostic method, ECLoss can be applied to various backbones of deep learning networks.
- 5) As an exploratory study, ECLoss achieved superior

explainability metrics, and improved the performance of face verification.

## 2. Related Work

### 2.1. Face Recognition

Face recognition has been studied for several decades. Before deep learning, many previous studies are based on feature engineering [9, 27, 6]. Due to the rapid development of deep learning, face recognition has made a huge achievement [70, 55, 56, 42, 57, 50, 60]. Sun *et al.* proposed a network to learn high-level feature representations through multi-class face identification tasks [55]. Taigman *et al.* proposed DeepFace, a nine-layer deep neural network, for large-scale face recognition [56]. Parkhi *et al.* constructed a deeper neural network named VGGFace and achieved high accuracy [42]. Wang *et al.* presented NormFace using normalized features for training, which achieved a higher accuracy than that without normalization [57]. Kim *et al.* presented GroupFace to improve the quality of the embedding vector by utilizing diverse group-aware representations.

Meanwhile, the loss function for face recognition has also been gradually improved [50, 60, 73, 34, 58, 14, 71, 17]. Schroff *et al.* proposed triplet loss to minimize the distance between an anchor and a positive sample of the same identity, and maximize the distance between the same anchor and a negative sample with different identity [50]. Wen *et al.* presented center loss to learn a center for each identity and penalizes the distances between the features and their corresponding identity centers [60]. Zheng *et al.* applied ring loss to constrain a scaled unit circle, while maintaining convexity [73].

Although these previous methods have reached significant performance in face recognition, the deep networks still performs in a back-box manner, as we don't know what information the networks have learned.

### 2.2. Explainability & Interpretability

The explainability and the discrimination power are two crucial properties of a deep network [3, 68]. At present, there is a trade-off between high explainability and strong discrimination power. Trough deep neural networks, high discrimination ability can be achieved but lack of the explainability [69].

**Post-hoc Explanation via Visualization.** Post-hoc explanation aims to provide an understanding of what knowledge has been learned by networks, in an intuitive manner of humans [16]. Visualization is the most direct and intuitive way to explore the pattern hidden inside the deep network. [66] and [53] are two contemporary works, which proposed deconvolutional methods for visualizing knowledge learned by networks. [53] presented an gradient-based image-specific

class saliency visualization method, which can visualize the spatial support of a particular class for a given input image. [37, 15] shows a visualization method by inverting the image representations, which can not only be used for deep neural networks, but also for deep neural networks, but also for various features, such as histogram of oriented gradients (HOG) [18, 12], local binary patterns (LBP) [41, 40] and scale invariant feature transform (SIFT) [36].

In addition, visualization methods based on Class Activation Maps (CAMs) are also emerging. CAM based method was first introduced in [76] to denote the discriminative regions of a particular category for a given input image. Subsequently, more and more improved CAMs, such as GradCAM [51], GradCAM++ [10], ScoreCAM [59] and so forth [47, 39], are proposed.

Specifically, in face recognition, [74] shows a method to find what difference between two similar-looking faces by a pair-wise patch-by-patch occlusion method, but it does not indicate what knowledge has been acquired by networks. [65] applied a CAMs method to generate heatmaps to indicate the active regions of different faces from different people; the results showed that the active regions tend to cover a whole face, so it does not provide useful information.

These post-hoc visualization methods have been successfully used in various fields of computer vision, like object classification [33], attacking [70], biometrics [46] and medical image processing [45], but they are difficult to generalize to face recognition. Therefore, model-intrinsic explanation methods are usually considered in face recognition.

**Model-intrinsic Explanation via Visualization.** Model-intrinsic explanations are often derived from intrinsic, transparent, or white-box models [31], which has simple structures, such as decision trees or linear models. In this paper, we mainly focus on the methods to improve the explainability of network. These models have better partial explainability, to some extent, than traditional models. [64] proposed a spatial diversity loss and a feature diversity loss to enhance explainable representations, which reach an outstanding performance on three face recognition benchmarks, but it requires occluded faces before training. [30] proposed a novel similarity metric, named explainable cosine (xCos), that can be plugged into various traditional networks to provide meaningful explanations on face recognition. Although it obtained comparable results, it did not reveal the knowledge learned inside the network.

In this study, we aim to constrain the deep network to learn an explainable facial part-based structural representation, without requirement for any manual annotation or occluded faces.

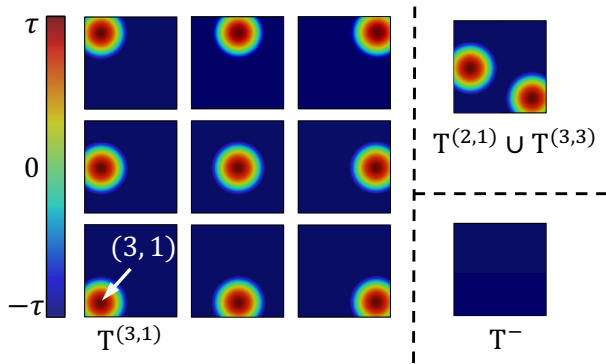


Figure 3. **(Left)** Examples of  $3 \times 3$  activation templates for ECLoss. **(Top-right)** An example template with two activation peaks. **(Bottom-right)** The negative template without any activation peak.

### 3. Method

In this study, our goal is to guide the network to learn a facial part-based structural representation. Formally, we need to match the activation peaks of feature maps with the face part of the input face. In object detection and classification, the object always occupies adjacent pixels in the picture, but in face recognition, the face part, such as two eyes may be separated. To go a step further, we proposed a loss function to guide each channel of the feature map to contain maximum two activation peaks, and make an individual channel learn the same semantic parts.

As shown in Figure 2-(a), our activation templates contain all possible variations of activation patterns in the feature maps, which have zero, one, or two activation peaks. As we know, the representation of initial deep learning networks without training is random. Even for a well trained network, its representation is usually mixed with high-dimensional abstract features that humans cannot understand.

In this study, the task of the proposed ECLoss is to match the feature maps of the target layer within the network with a subset of activation templates  $\mathbb{T}$ . Therefore, we extend the definitions of mutual information in information theory from variable to sets of variables, which is a measure of the mutual dependence between the two sets. Our proposed ECLoss enables the network to learn the representation of activation templates by increasing the mutual information between activation templates and feature maps of the network. As shown in Figure 2-(c), our proposed ECLoss is applied to the last convolutional layer of the network to increase the mutual information  $MI(\mathbb{T}; \mathbb{X})$  between activation templates  $\mathbb{T}$  and feature maps  $\mathbb{X}$ . As a result, after training, the patterns of the feature maps  $\mathbb{X}$  will match the activation templates  $\mathbb{T}$ .

The proposed ECLoss is a generic and model-agnostic method that can be used for various face recognition networks. For example, Figure 2-(c) shows that our generic

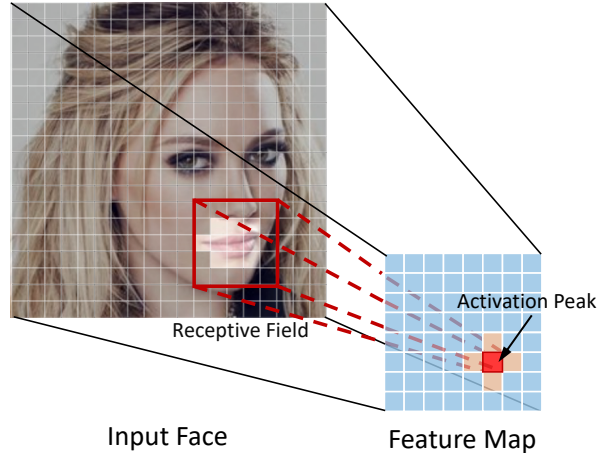


Figure 4. Assuming that the face part of interest is the mouth, the pixels of the feature map corresponding to the mouth in its receptive field will be activated.

channel loss function works on the last layer of the encoder, and can be used with other loss functions. Formally, in this work, our total loss function is defined as:

$$\text{Total Loss} = \alpha \text{Loss}(y, \hat{y}) + \beta \text{ECLoss} \quad (1)$$

where  $\text{Loss}(y, \hat{y})$  indicates the loss between true subject ID label and the prediction, the  $\alpha$  and  $\beta$  are weighting coefficients.

#### 3.1. Activation Templates

Given the face images  $I$  with the size  $s \times s$  as the input, the face recognition network with parameter  $\theta$  can represent  $I$  as the feature maps  $\mathbb{X}$  from the target convolutional layer. In particular,  $\mathbb{X} = \{x_1, x_2, \dots, x_i, \dots, x_c\}$ , where  $x_i$  refers to the  $i$ -th channel of  $\mathbb{X}$ .

**Activation templates with one peak.** For an unknown face, the face parts may appear in any pixel of the input face image, *i. e.*, any pixel of the feature map may be activated if there is a face part of interest in the receptive field, as shown in Figure 4.

Let  $T^{(i,j)}$  denotes the activation template containing an activation peak in coordinate  $(i, j)$ , and  $T_{(u,v)}^{(i,j)}$  indicates the value in coordinate  $(u, v)$  of the activation template  $T^{(i,j)}$ . For each activation template, the value of the activation peak is  $\tau$  and the value of other pixels extend outward the peak is defined as:

$$T_{(u,v)}^{(i,j)} = \tau \cdot \max\left(1 - \frac{\|(u,v) - (i,j)\|_2}{r}, -1\right) \quad (2)$$

where the  $\tau$  is a constant greater than 0,  $\|\cdot\|_2$  denote  $L2$ -Norm distance,  $r$  is a constant that denotes the radius of the area

greater than 0. To go a step further, the one-peak activation template set  $\mathbb{T}_1$  is defined as  $\mathbb{T}_1 = \{ \mathbf{T}^{(i,j)} \mid 1 \leq i, j \leq s \}$ .

In addition, a negative template  $\mathbf{T}^-$  is defined to represent a feature map without any activation peaks,  $\mathbf{T}^-_{(i,j)} = -\tau$  for every coordinate  $(i, j)$  within the template  $\mathbf{T}^-$ .

**Activation templates with two peaks.** In order to match activation peaks with face parts, we allow a feature map to contain at most two activation peaks. In this situation, we define the two-peak templates to be the combination of any two one-peak templates, as shown in Figure 2. The combination  $\mathbf{T}^{(i_1, j_1)} \cup \mathbf{T}^{(i_2, j_2)}$  of two one-peak templates  $\mathbf{T}^{(i_1, j_1)}$  and  $\mathbf{T}^{(i_2, j_2)}$  is defined as:

$$\mathbf{T}_{(u,v)} = \max(\mathbf{T}^{(i_1, j_1)}_{(u,v)}, \mathbf{T}^{(i_2, j_2)}_{(u,v)}) \quad (3)$$

where  $\mathbf{T}_{(u,v)}$  is a two-peak template combining two one-peak template  $\mathbf{T}^{(i_1, j_1)}_{(u,v)}$  and  $\mathbf{T}^{(i_2, j_2)}_{(u,v)}$ . Then, the two-peak template set  $\mathbb{T}_2$  is defined as:

$$\mathbb{T}_2 = \left\{ \mathbf{T}^{(i_1, j_1)} \cup \mathbf{T}^{(i_2, j_2)} \mid 1 \leq i_1, i_2, j_1, j_2 \leq s \right\} \quad (4)$$

As shown in Figure 2, a set of activation templates  $\mathbb{T}$  used for ECLoss contain all of the one-peak templates, two-peak templates and a negative template  $\mathbf{T}^-$ ,  $\mathbb{T} = \mathbb{T}_1 \cup \mathbb{T}_2 \cup \{\mathbf{T}^-\}$ .

### 3.2. Explainable Channel Loss

In this study, our major goal is to make each dimension of the representation tend to represent a face part. Generally, before training, the feature maps is a random output when the input face images go through the network, so the feature maps  $\mathbb{X}$  and the locations of all face parts are unrelated. In this case, after network training, each dimension of the feature map belonging to  $\mathbb{X}$  will be able to match activation templates  $\mathbb{T}$ .

**Problem Definition:** Given a template set of activation pattern  $\mathbb{T}$ , and a feature map  $\mathbb{X}$  of the target convolutional layer from the face recognition network, the task of ECLoss is to find parameters  $\theta$  such that feature map  $\mathbb{X}$  maximally represent a subset of the face part set  $\mathbb{X}$ .

By extending the definitions of mutual information in information theory from variable to sets of variables [7, 26], the mutual information between  $\mathbb{X}$  and  $\mathbb{T}$  is defined as:

$$\begin{aligned} \text{MI}(\mathbb{T}; \mathbb{X}) &= \sum_{\mathbf{T} \in \mathbb{T}} \sum_{x \in \mathbb{X}} P(\mathbf{T}, x) \log\left(\frac{P(\mathbf{T}, x)}{P(\mathbf{T})P(x)}\right) \\ &= \sum_{\mathbf{T} \in \mathbb{T}} \sum_{x \in \mathbb{X}} P(x)P(\mathbf{T}|x) \log\left(\frac{P(\mathbf{T}|x)}{P(\mathbf{T})}\right) \end{aligned} \quad (5)$$

where  $P(\mu)$  represents the prior probability of a activation template from  $\mathbb{T}$ .  $P(x)$  denotes the probability of

appearance of feature maps of different patterns,  $P(x) = \sum_{\mathbf{T} \in \mathbb{T}} P(\mathbf{T})P(x|\mathbf{T})$ . To simplify the problem, we assume that all templates are uniformly distributed, so the  $P(\mathbf{T})$  is given as a constant of  $\frac{1}{|\mathbb{T}|}$ .  $P(\mathbf{T}|x)$  is the conditional likelihood denoting the fitness between  $\mathbf{T}$  and  $x$ :

$$P(\mathbf{T}|x) = \frac{e^{tr(x \cdot \mathbf{T})}}{\sum_{\hat{\mathbf{T}} \in \mathbb{T}} e^{tr(x \cdot \hat{\mathbf{T}})}} \quad (6)$$

where  $\cdot$  indicates hadamard product (element-wise product),  $tr(\ast)$  indicates the trace of a matrix, so  $tr(x \cdot \mathbf{T})$  can be rewritten as  $tr(x \cdot \mathbf{T}) = \sum_i \sum_j x_{ij} \mathbf{T}_{ij}$ .

To increase the mutual information between  $\mathbb{T}$  and  $\mathbb{X}$ , ECLoss is defined as  $\text{ECLoss} = -\text{MI}(\mathbb{T}; \mathbb{X})$ . Then, the total loss function is defined as:

$$\text{Total Loss} = \alpha \text{Loss}(y, \hat{y}) - \beta \text{MI}(\mathbb{T}; \mathbb{X}) \quad (7)$$

### 3.3. Visualization of Structural Representation

Given the face images  $I$  with the size  $s \times s$  as the input, the face recognition network with parameter  $\theta$  can represent  $I$  as the feature maps  $\mathbb{X}$  from the target convolutional layer after the ReLU operation. In particular,  $\mathbb{X} = \{x_1, x_2, \dots, x_i, \dots, x_c\}$ , where  $x_i$  refers to the  $i$ -th channel of  $\mathbb{X}$ . The feature map  $x$  is a  $n \times n$  matrix encoded by the face recognition network. In order to ensure the same resolution of  $x$  as the input face, feature map  $x$  will be resized to  $s \times s$  by bi-linear upsampling.

To focus on the area of maximum activation, the area of top 10% intensity will be highlighted, while other area will be discarded. A threshold  $t$  is found to highlight the area of top 10% intensity in the feature map  $x$ :

$$\hat{x}_{(i,j)} = \begin{cases} x_{(i,j)}, & x_{(i,j)} \geq t \\ 0, & \text{otherwise} \end{cases} \quad (8)$$

Then the threshold  $t$  is defined as:

$$\hat{t} \equiv \arg \max_t \left\{ P(\hat{x}_{(i,j)} > t) \geq 0.1 \right\} \quad (9)$$

where  $P$  is the probability when the condition is true. Some examples of visualization for top 10% activation are shown on Figure 6, which are the result of transforming  $\hat{x}$  into the heatmap style and superimposing it on the original face image.

## 4. Experiment

### 4.1. Dataset & Pre-processing

**Training Dataset** The Glint360K [1] is a large scale dataset merged from Celeb-500K [8] and MS-Celeb-1M [20], containing 17 million face images from 360K individuals. All face images of the Glint360K are downloaded from Internet

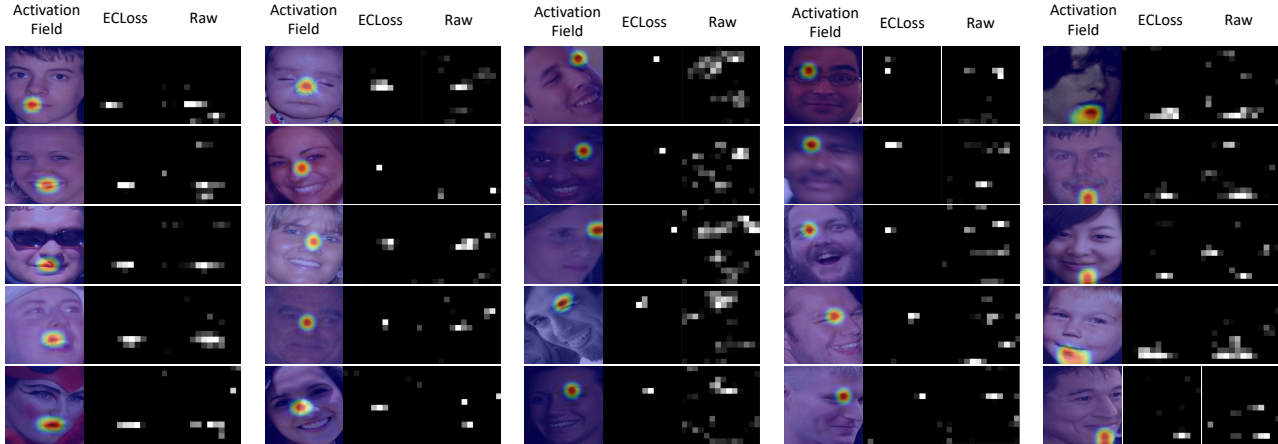


Figure 5. Comparison of the feature map between networks with and without ECLoss. For the same input face, the feature map of the explainable network trained with ECLoss has at most two activation peaks, and usually activates a certain face part. Instead, the feature map of the original network has more noises, and the activation peaks are located randomly on different parts.

and then pre-processed to size of  $112 \times 112$  by 5 facial marks predicted by the face localisation method RetinaFace [13].

**Testing Dataset** For testing robustness of face recognition, we explore various face verification datasets: LFW [22], CFP-FF [52] and CALFW [72]. Besides, in this study, many explainability metrics are assessed using several datasets, such as VGGFace[42], AgeDB [38], Helen [28], 300-W[48], LaPa [35], AFW [77] and LFPW [5, 49]. All datasets used in training and testing are listed in Table 1.

Table 1. The list of face datasets used for training and testing

Stage	Dataset	Landmark Pose	Image / Pairs
Training	Glint360K [1]	- Near-frontal	17,091,657 / -
	LFW [22]	- Near-frontal	- / 6,000
	CFP-FF [52]	- Near-frontal	- / 7,000
	CALFW [72]	- Near-frontal	- / 3,000
	VGGFace [42]	- Near-frontal	982,803 / -
Testing	AgeDB [38]	- Near-frontal	16, 488 / -
	300-W [48]	68 Near-frontal	3,148 / -
	AFW [77]	68 $[-45^\circ, 45^\circ]$	750,000 / -
	Helen [28]	68 $[-90^\circ, 90^\circ]$	2,000 / -
	LaPa [35]	106 $[-90^\circ, 90^\circ]$	22,000 / -
	LFPW [5]	68 $[-90^\circ, 90^\circ]$	1,432 / -

**Pre-processing** Different faces have almost the same

characteristics, such as the position, size and shape of facial components. For face recognition, face alignment is an essential prerequisite, which can align facial components, e.g., eye, nose, mouth, and contour to a standard facial space. In this study, in order to reduce the influence of the structural representation by the standard facial space, the data used for training and testing are not aligned. All face images used for training and testing are detected and cropped by MTCNN [62], and resized to  $224 \times 224$ .

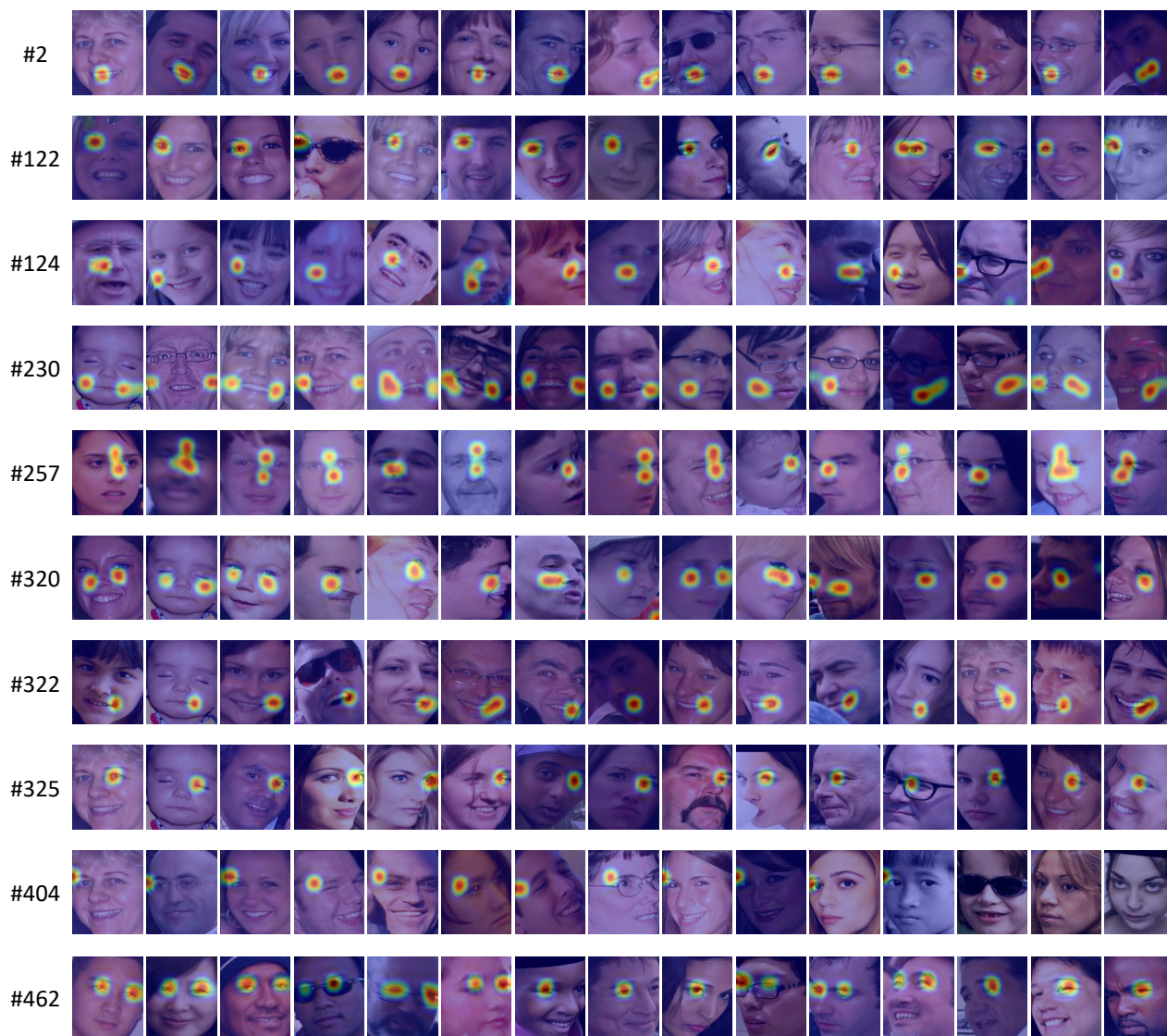
## 4.2. Implementation Details

We trained three explainable networks based on VGG13 [54], VGG16 [54], and VGG19 [54] for face recognition in the Glint-360K dataset. And original VGG13, VGG16, and VGG19 were trained on the same dataset and settings for comparison. As the skip connections of the residual networks mix different pattern of multiple layers in a single feature map [21, 67], we do not use residual networks and skip connection in this study. In these experiments, the input face images are detected by MTCNN and resized to  $224 \times 224$ , without any face alignment.

For activation templates, we found in our experiments that the results are not sensitive to the value of  $\tau$ . As ECLoss might overflow when the value of  $\tau$  is big, we set  $\tau$  to a small number, *i.e.*  $t = 0.001$ , and  $r = 4$ . For total loss function of  $\text{Total Loss} = \alpha \text{Loss}(y, \hat{y}) - \beta \text{MI}(\mathbb{T}; \mathbb{X})$ , we set the  $\alpha$  as a constant of 1, and  $\beta$  is set as  $1e^{-5}$  initially and then automatically changed by the program to reduce the total loss.

In the VGG architecture, the shape of last convolutional layer is  $14 \times 14$ , *i.e.*, for each channel, tens of thousands of activation templates can be generated (nearly  $14^4$  two-peak templates,  $14^2$  one-peak templates and 1 negative template).

### Visualization of channels of network trained with ECLoss



---

### Visualization of channels of network trained without ECLoss



Figure 6. Visualization for top 10% activation. **(Top)** The activation peaks of an individual channel tend to be located in the same face part, and each channel of feature maps contains at most two activation peaks. **(Bottom)** Almost all feature maps that contain more than two activation peaks, the activation peaks have no specific meaning for face recognition.

To reduce the complexity of calculation, we take 400 templates evenly from original template set  $\mathbb{T}^{ori}$  as a new set  $\mathbb{T}$  used for all experiments.

For mutual information  $MI(\mathbb{T}; \mathbb{X})$  between  $\mathbb{T}$  and  $\mathbb{X}$ , we assume that all templates of  $\mathbb{T}$  are uniformly distributed, so we set  $|\mathbb{T}| = 400$ ,  $P(\mathbb{T}) = \frac{1}{|\mathbb{T}|} = 0.0025$ . Because  $P(x) = \sum_{\mathbb{T}} P(\mathbb{T})P(x|\mathbb{T})$ ,  $\mathbb{T} \in \mathbb{T}$  is computed using numerous prior feature map requiring large amounts of memory. we approximate  $P(x)$  as  $\sum_{\mathbb{T}} P(\mathbb{T})E_x \left[ \frac{e^{tr(x \cdot \mathbb{T})}}{\sum_{\hat{\mathbb{T}}} e^{tr(x \cdot \hat{\mathbb{T})}} \right]$ , where  $E[\cdot]$  indicates the mathematic expectation,  $tr(\cdot)$  indicates the trace of a matrix, and  $P(\mathbb{T}) = 0.0025$ .

All experiments are conducted on a workstation with eight NVIDIA Tesla V100 GPUs. Moreover, the learning rate is set to 0.03 and the batch size is set to 64.

## 5. Result & Analysis

### 5.1. Visualization of Activation

As mentioned in the section 3.3, we visualized the receptive fields of activation of a channel. Previous studies in [3, 75] and [68] have introduced this method to compute the receptive fields on a given feature map.

For both networks trained with and without ECLoss, we visualize the top 10% activation values of the last convolutional layer. As shown in Figure 6, the maximal activation area in the network trained with ECLoss can focus on a certain facial part, like face, cheek, nose, *etc.*, but the original network randomly focus on some unexplainable semantic information. Moreover, for explainable networks trained with ECLoss, these clear disentanglements of structural part-based representation can easily help people to know what knowledge the network has learned, which is helpful for quantifying the contribution of different face parts to the network.

We found that, within the explainable face recognition networks trained with ECLoss, an individual layer usually detected a certain face part even if the input face images are from different people. For example, as shown in Figure 6, the 2nd channel detected the mouth, the 122nd channel detected the left eye, the 257th channel detected the nose, the 325th channel detected the right eye, the 462nd channel detected the eyes, *etc.* In addition, it not only detected face components, but also learned some patterns that make sense to the network. For example, the 124th channel learned the area to the right of the nose, and the 404th channel learned the area to the right of the right eye.

In addition, we also compare the feature map of the explainable network and the original network in Figure 5. Given the same face as input, our explainable networks usually have at most two activation peaks in a feature map, and the activation peaks tend to activate a certain face part. Instead, the activation peaks of the feature map of the original

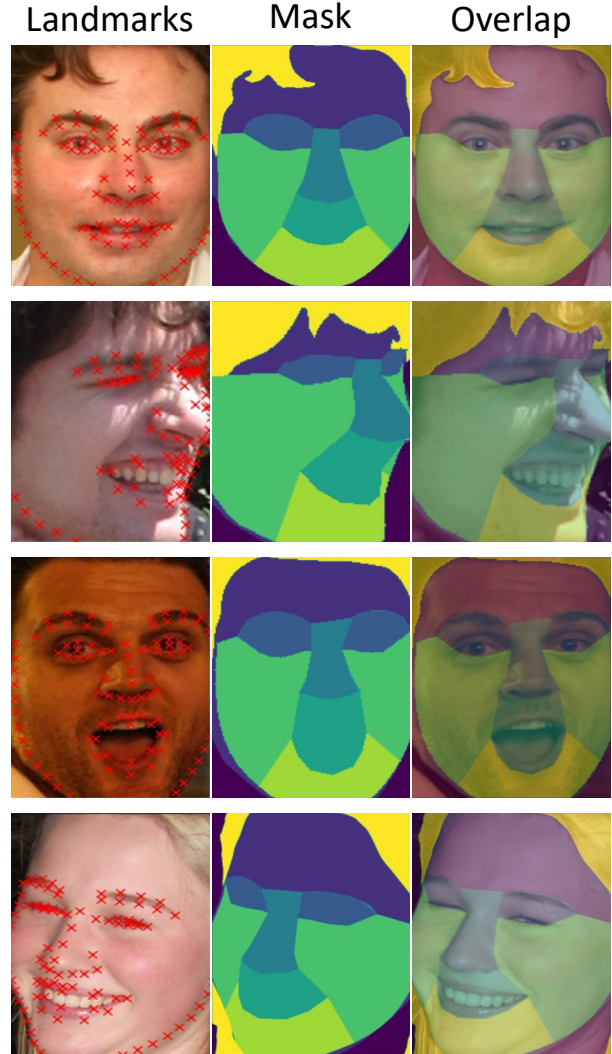


Figure 7. Re-annotation by landmarks for evaluation of part explainability. **(Left Column)** Original landmarks on face from face parsing dataset. **(Middle Column)** Re-annotation mask by landmarks containing hair, forehead, cheek, eyes, nose, mouth and jaw. **(Right Column)** Visualization of mask overlapped the face.

network usually contain a lot of noises, and are randomly located on different areas.

### 5.2. Quantitative Analysis

#### 5.2.1 Face Verification

Face verification mainly computes the similarity between a reference and a probe face image to decide if these face images are of the same identity [11]. In the evaluation of face verification, LFW [22], CFP-FF [52] and CALFW [72] datasets are used to assess performance of the explainable face recognition networks and the original networks.

In all experiments, we did not perform face alignment.



Table 2. The evaluation metric of part explainability on various dataset: LaPa, AFW, Helen, LFPW and 300-W.

Network	LaPa	AFW	Helen	LFPW	300-W
VGG13 + Softmax	0.1642	0.1612	0.1646	0.1625	0.1554
VGG13 + ECLoss	<b>0.1710</b>	<b>0.1687</b>	<b>0.1711</b>	<b>0.1702</b>	<b>0.1623</b>
VGG16 + Softmax	0.1479	0.1447	0.1530	<b>0.1443</b>	0.1396
VGG16 + ECLoss	<b>0.1632</b>	<b>0.1490</b>	<b>0.1566</b>	0.1431	<b>0.1443</b>
VGG19 + Softmax	0.0424	0.0396	0.0396	0.0376	0.0381
VGG19 + ECLoss	<b>0.0432</b>	<b>0.0426</b>	<b>0.0466</b>	<b>0.0430</b>	<b>0.0376</b>

As shown in Table 2, compared to the original networks, the explainable network with the proposed ECLoss attained a significant improvement. The VGG13 network trained with ECLoss achieved 0.2%, 0.13% and 0.58% higher accuracy on LFW, CFP-FF, and CALFW datasets, respectively. The results of VGG16 with ECLoss are 0.88%, 2.08% and 2.6% higher than the original network. The accuracy of VGG19 with ECLoss is 0.79%, 0.26% and 5.01% higher than the original network.

Table 3. Face verification accuracy on LFW, CFP-FF and CALFW datasets without face alignment. Compared to the original networks, the explainable network with the proposed ECLoss achieves a significant improvement.

Network	LFW	CFP-FF	CALFW
VGG13 + Softmax	91.95%	79.57%	76.55%
VGG13 + ECLoss	<b>92.15%</b>	<b>79.70%</b>	<b>77.13%</b>
VGG16 + Softmax	93.20%	78.59%	78.10%
VGG16 + ECLoss	<b>94.08%</b>	<b>80.67%</b>	<b>80.70%</b>
VGG19 + Softmax	90.96%	75.90%	70.97%
VGG19 + ECLoss	<b>91.75%</b>	<b>76.16%</b>	<b>75.98%</b>

### 5.2.2 Part Explainability

This evaluation metric of part explainability was proposed by Bau *et al.* [3] and Zhang *et al.* [68], which measures the object-part explainability of channels from a network.

For assessing part explainability of various network, five face parsing datasets of LaPa [35], AFW [77], Helen [28], LFPW [5] and 300-W [48] datasets are used. The details of these datasets are shown in Table 1. Before evaluation of part explainability, as shown in Figure 7, we generate facial

component masks for these face datasets by their landmarks, which contain hair, forehead, cheek, eyes, nose, mouth, and jaw. Formally, a facial components set is defined as  $\mathbb{K} = \{\text{hair, forehead, cheek, etc.}\}$ .

Given a face recognition network, let  $I$  denote the face image input to the network,  $x$  represents a channel of the feature maps  $\mathbb{X}$  from the last convolutional layer of the encoder after the activation function of ReLU. The feature map  $x$  is first resized to  $s \times s$  by bi-linear upsampling, where  $s$  is the size of the input image. A threshold  $t$  is then applied to find out the top 10% activation area using Equation (9). Then, the fitness of feature map  $x$  regarding to the facial component  $k \in \mathbb{K}$  is computed by

$$\text{IoU}_{\text{Mask}_k, x} = \frac{\text{P}[\text{Mask}_k \cap x]}{\text{P}[\text{Mask}_k \cup x]} \quad (10)$$

where  $\text{P}$  is the probability when the condition is true, and  $\text{Mask}_k$  is the binary mask that represents the ground-truth of the facial component  $k$ , which is derived from our re-annotation of various component datasets shown on Figure 7.

For evaluation of part explainability, we compute  $\text{PE}_I = \mathbf{E}_{x \in \mathbb{X}} [\max_k (\text{IoU}_{\text{Mask}_k, x})]$  for each input face image. As shown on Table 2, for each network, we conduct several independent experiments, where a random selection of 100 face images from each face parsing dataset is used to calculate the part explainability.

### 5.2.3 Location Consistency

The metrics of location consistency assess the consistency of the location of the activation peaks [68, 3], which indicate whether the channel of feature maps is able to detect the same face part regardless of the input image, as shown in Figure 6.

For evaluation of location consistency, we first find the face component  $\hat{k}$  with maximum correspondence by  $\hat{k} = \arg \max_k (\text{IoU}_{\text{Mask}_k, x})$ . Therefore, for the  $i$ -th channel of

Table 4. The evaluation metric of location consistency on various dataset: LaPa, AFW, Helen, LFPW and 300-W.

Network	LaPa	AFW	Helen	LFPW	300-W
VGG13 + Softmax	0.02537	0.01971	0.02082	0.02187	0.02122
VGG13 + ECLoss	<b>0.04029</b>	<b>0.03654</b>	<b>0.03661</b>	<b>0.03796</b>	<b>0.03770</b>
VGG16 + Softmax	0.02743	0.03516	0.03032	<b>0.04230</b>	0.02867
VGG16 + ECLoss	<b>0.02898</b>	<b>0.03589</b>	<b>0.03327</b>	0.04175	<b>0.03417</b>
VGG19 + Softmax	0.08075	0.08307	0.08767	0.08217	0.08450
VGG19 + ECLoss	<b>0.09382</b>	<b>0.09503</b>	<b>0.09592</b>	<b>0.09453</b>	<b>0.09418</b>

Table 5. The evaluation metric of **activation robustness** (Means  $\pm$  Standard Error) on various dataset: VGGFace, LFW, CFP, AgeDB, Helen and LaPa.

Network	VGGFace	LFW	CFP	AgeDB	Helen	LaPa
VGG13 + Softmax	3.733 $\pm$ 0.094	3.945 $\pm$ 0.022	3.580 $\pm$ 0.205	3.984 $\pm$ 0.147	4.070 $\pm$ 0.164	3.918 $\pm$ 0.236
VGG13 + ECLoss	<b>2.596 <math>\pm</math> 0.050</b>	<b>2.784 <math>\pm</math> 0.077</b>	<b>2.495 <math>\pm</math> 0.126</b>	<b>2.718 <math>\pm</math> 0.221</b>	<b>2.816 <math>\pm</math> 0.105</b>	<b>2.889 <math>\pm</math> 0.166</b>
VGG16 + Softmax	3.714 $\pm$ 0.081	3.994 $\pm$ 0.041	3.994 $\pm$ 0.041	3.889 $\pm$ 0.167	3.946 $\pm$ 0.144	3.847 $\pm$ 0.195
VGG16 + ECLoss	<b>3.144 <math>\pm</math> 0.086</b>	<b>3.272 <math>\pm</math> 0.013</b>	<b>3.210 <math>\pm</math> 0.078</b>	<b>3.429 <math>\pm</math> 0.165</b>	<b>3.242 <math>\pm</math> 0.151</b>	<b>3.395 <math>\pm</math> 0.186</b>
VGG19 + Softmax	2.987 $\pm$ 0.111	2.965 $\pm$ 0.247	2.646 $\pm$ 0.069	3.053 $\pm$ 0.123	3.083 $\pm$ 0.148	3.068 $\pm$ 0.042
VGG19 + ECLoss	<b>1.672 <math>\pm</math> 0.108</b>	<b>1.743 <math>\pm</math> 0.164</b>	<b>1.493 <math>\pm</math> 0.037</b>	<b>1.775 <math>\pm</math> 0.183</b>	<b>1.829 <math>\pm</math> 0.053</b>	<b>1.849 <math>\pm</math> 0.065</b>

feature maps  $x_i$ , we compute its corresponding face part  $\hat{k}$  for different input images  $I$ .

Given a channel’s index  $i$ ,  $A_{i,k}$  indicates the probability of the feature map  $x_i$  corresponding to the  $k$ -th face part,  $i$ . *e.*, for an arbitrary channel’s index  $i$ ,  $\sum_{k \in \mathbb{K}} A_{i,k} = 1$ . For the  $i$ -th channel, we use  $S_i = \text{var}[A_{i,k}] = \frac{\sqrt{\sum_{k \in \mathbb{K}} (A_{i,k} - \frac{1}{|\mathbb{K}|})^2}}{|\mathbb{K}|}$ ,  $k \in \mathbb{K}$  to assess its consistency. For a network architecture, we use  $LS = \mathbf{E}[S_i] = \frac{\sum_{i=1}^c S_i}{c}$  to evaluate location consistency of the network.

The results are shown in Table 4. For each network, we conduct several independent experiments, using a random selection of 100 face images from each face parsing dataset (LaPa [35], AFW [77], Helen [28], LFPW [5] and 300-W [48]).

#### 5.2.4 Activation Robustness

The main goal of the proposed ECLoss is to force a feature map to contain at most two activation peaks. As shown in Figure 6 and Figure 5, compared to the feature maps of explainable networks trained with ECLoss, the feature maps of original networks usually involve more than two activation

peaks. Therefore, when the number of activation peaks is smaller, the activation pattern is more robust.

In simple terms, the purpose of Activation Robustness is to evaluate the average number of peaks in the feature map. Given a feature map  $x$  after ReLU operation from the last convolutional layer. Then, a contour method [44, 43] will be used to compute peak prominence on the feature map  $x$ , which uses enclosing contours to define the local maxima.

In the experiments of activation robustness, for VGG13, VGG16, VGG19, explainable VGG13, explainable VGG16, and explainable VGG19, we conduct 5 independent experiments to calculate the mean and standard deviation of the number of activation peaks. The results of these experiments have been shown in Table 5, which demonstrate that our proposed ECLoss achieves better robustness on the six datasets of VGGFace [42], LFW [22], CFP [52], AgeDB [38], Helen [28] and LaPa [35].

## 6. Conclusion

In this paper, we proposed an Explainable Channel Loss (ECLoss) to construct an explainable face recognition network by forcing the target convolution layer to learn the

facial part-based representation. Each channel of the feature maps represents a certain face part, without any manual annotation or additional occlusion datasets. We assess the proposed ECLoss by three traditional deep learning architectures VGG13 [54], VGG16 [54], and VGG19 [54] on dozens of datasets like Glint360K [1], LFW [22], CFP [52], CALFW [72], VGGFace [42], AgeDB [38], 300-W [48], AFW [77], Helen [28], LaPa [35] and LFPW [5]. All of our experiments have shown that our proposed ECLoss can achieve significant explainability metrics while improving the performance of face recognition.

## 7. Acknowledgements

This research was supported by National Natural Science Foundation of China under grant no. 91959108.

## References

- [1] Xiang An, Xuhan Zhu, Yuan Gao, Yang Xiao, Yongle Zhao, Ziyong Feng, Lan Wu, Bin Qin, Ming Zhang, Debing Zhang, et al. Partial fc: Training 10 million identities on a single machine. In *Proceedings of the IEEE/CVF International Conference on Computer Vision*, pages 1445–1449, 2021.
- [2] Sebastian Bach, Alexander Binder, Grégoire Montavon, Frederick Klauschen, Klaus-Robert Müller, and Wojciech Samek. On pixel-wise explanations for non-linear classifier decisions by layer-wise relevance propagation. *PLoS one*, 10(7):e0130140, 2015.
- [3] David Bau, Bolei Zhou, Aditya Khosla, Aude Oliva, and Antonio Torralba. Network dissection: Quantifying interpretability of deep visual representations. In *Proceedings of the IEEE conference on computer vision and pattern recognition*, pages 6541–6549, 2017.
- [4] David Bau, Jun-Yan Zhu, Hendrik Strobelt, Agata Lapedriza, Bolei Zhou, and Antonio Torralba. Understanding the role of individual units in a deep neural network. *Proceedings of the National Academy of Sciences*, 117(48):30071–30078, 2020.
- [5] Peter N Belhumeur, David W Jacobs, David J Kriegman, and Neeraj Kumar. Localizing parts of faces using a consensus of exemplars. *IEEE transactions on pattern analysis and machine intelligence*, 35(12):2930–2940, 2013.
- [6] Thomas Berg and Peter N Belhumeur. Poof: Part-based one-vs.-one features for fine-grained categorization, face verification, and attribute estimation. In *Proceedings of the IEEE Conference on Computer Vision and Pattern Recognition*, pages 955–962, 2013.
- [7] Leon Brillouin. *Science and information theory*. Courier Corporation, 2013.
- [8] Jiajiong Cao, Yingming Li, and Zhongfei Zhang. Celeb-500k: A large training dataset for face recognition. In *2018 25th IEEE International Conference on Image Processing (ICIP)*, pages 2406–2410. IEEE, 2018.
- [9] Zhimin Cao, Qi Yin, Xiaoou Tang, and Jian Sun. Face recognition with learning-based descriptor. In *2010 IEEE Computer society conference on computer vision and pattern recognition*, pages 2707–2714. IEEE, 2010.
- [10] Aditya Chattopadhyay, Anirban Sarkar, Prantik Howlader, and Vineeth N Balasubramanian. Grad-cam++: Generalized gradient-based visual explanations for deep convolutional networks. In *2018 IEEE winter conference on applications of computer vision (WACV)*, pages 839–847. IEEE, 2018.
- [11] Nate Crosswhite, Jeffrey Byrne, Chris Stauffer, Omkar Parkhi, Qiong Cao, and Andrew Zisserman. Template adaptation for face verification and identification. *Image and Vision Computing*, 79:35–48, 2018.
- [12] Navneet Dalal and Bill Triggs. Histograms of oriented gradients for human detection. In *2005 IEEE computer society conference on computer vision and pattern recognition (CVPR'05)*, volume 1, pages 886–893. Ieee, 2005.
- [13] Jiankang Deng, Jia Guo, Evangelos Ververas, Irene Kotsia, and Stefanos Zafeiriou. Retinaface: Single-shot multi-level face localisation in the wild. In *Proceedings of the IEEE/CVF Conference on Computer Vision and Pattern Recognition*, pages 5203–5212, 2020.
- [14] Jiankang Deng, Jia Guo, Niannan Xue, and Stefanos Zafeiriou. Arcface: Additive angular margin loss for deep face recognition. In *Proceedings of the IEEE/CVF Conference on Computer Vision and Pattern Recognition*, pages 4690–4699, 2019.
- [15] Alexey Dosovitskiy and Thomas Brox. Inverting visual representations with convolutional networks. In *Proceedings of the IEEE conference on computer vision and pattern recognition*, pages 4829–4837, 2016.
- [16] Mengnan Du, Ninghao Liu, and Xia Hu. Techniques for interpretable machine learning. *Communications of the ACM*, 63(1):68–77, 2019.
- [17] Yueqi Duan, Jiwen Lu, and Jie Zhou. Uniformface: Learning deep equidistributed representation for face recognition. In *Proceedings of the IEEE/CVF Conference on Computer Vision and Pattern Recognition*, pages 3415–3424, 2019.
- [18] Pedro F Felzenszwalb, Ross B Girshick, David McAllester, and Deva Ramanan. Object detection with discriminatively trained part-based models. *IEEE transactions on pattern analysis and machine intelligence*, 32(9):1627–1645, 2009.
- [19] Ruth C Fong and Andrea Vedaldi. Interpretable explanations of black boxes by meaningful perturbation. In *Proceedings of the IEEE international conference on computer vision*, pages 3429–3437, 2017.
- [20] Yandong Guo, Lei Zhang, Yuxiao Hu, Xiaodong He, and Jianfeng Gao. Ms-celeb-1m: A dataset and benchmark for large-scale face recognition. In *European conference on computer vision*, pages 87–102. Springer, 2016.
- [21] Kaiming He, Xiangyu Zhang, Shaoqing Ren, and Jian Sun. Deep residual learning for image recognition. In *Proceedings of the IEEE conference on computer vision and pattern recognition*, pages 770–778, 2016.
- [22] Gary B Huang, Marwan Mattar, Tamara Berg, and Eric Learned-Miller. Labeled faces in the wild: A database for studying face recognition in unconstrained environments. In *Workshop on faces in 'Real-Life' Images: detection, alignment, and recognition*, 2008.
- [23] Xiaobin Huang, Jingtian Xia, and Linlin Shen. One-class face anti-spoofing based on attention auto-encoder. In *Chi-*

- nese Conference on Biometric Recognition, pages 365–373. Springer, 2021.
- [24] Changyuan Jiang, Shisong Lin, Wei Chen, Feng Liu, and Linlin Shen. Pointface: Point set based feature learning for 3d face recognition. In *2021 IEEE International Joint Conference on Biometrics (IJCB)*, pages 1–8. IEEE, 2021.
- [25] Yonghyun Kim, Wonpyo Park, Myung-Cheol Roh, and Jongju Shin. Groupface: Learning latent groups and constructing group-based representations for face recognition. In *Proceedings of the IEEE/CVF Conference on Computer Vision and Pattern Recognition*, pages 5621–5630, 2020.
- [26] Solomon Kullback. *Information theory and statistics*. Courier Corporation, 1997.
- [27] Neeraj Kumar, Alexander C Berg, Peter N Belhumeur, and Shree K Nayar. Attribute and simile classifiers for face verification. In *2009 IEEE 12th international conference on computer vision*, pages 365–372. IEEE, 2009.
- [28] Vuong Le, Jonathan Brandt, Zhe Lin, Lubomir Bourdev, and Thomas S Huang. Interactive facial feature localization. In *European conference on computer vision*, pages 679–692. Springer, 2012.
- [29] Tsung-Yi Lin, Piotr Dollár, Ross Girshick, Kaiming He, Bharath Hariharan, and Serge Belongie. Feature pyramid networks for object detection. In *Proceedings of the IEEE conference on computer vision and pattern recognition*, pages 2117–2125, 2017.
- [30] Yu-Sheng Lin, Zhe-Yu Liu, Yu-An Chen, Yu-Siang Wang, Ya-Liang Chang, and Winston H Hsu. xcos: An explainable cosine metric for face verification task. *ACM Transactions on Multimedia Computing, Communications, and Applications (TOMM)*, 17(3s):1–16, 2021.
- [31] Pantelis Linardatos, Vasilis Papastefanopoulos, and Sotiris Kotsiantis. Explainable ai: A review of machine learning interpretability methods. *Entropy*, 23(1):18, 2021.
- [32] Haozhe Liu, Haoqin Ji, Yuexiang Li, Nanjun He, Haoqian Wu, Feng Liu, Linlin Shen, and Yefeng Zheng. Robust representation via dynamic feature aggregation. *arXiv preprint arXiv:2205.07466*, 2022.
- [33] Haozhe Liu, Haoqian Wu, Weicheng Xie, Feng Liu, and Linlin Shen. Group-wise inhibition based feature regularization for robust classification. *arXiv preprint arXiv:2103.02152*, 2021.
- [34] Weiyang Liu, Yandong Wen, Zhiding Yu, Ming Li, Bhiksha Raj, and Le Song. Spheroface: Deep hypersphere embedding for face recognition. In *Proceedings of the IEEE conference on computer vision and pattern recognition*, pages 212–220, 2017.
- [35] Yinglu Liu, Hailin Shi, Hao Shen, Yue Si, Xiaobo Wang, and Tao Mei. A new dataset and boundary-attention semantic segmentation for face parsing. In *AAAI*, pages 11637–11644, 2020.
- [36] David G Lowe. Distinctive image features from scale-invariant keypoints. *International journal of computer vision*, 60(2):91–110, 2004.
- [37] Aravindh Mahendran and Andrea Vedaldi. Understanding deep image representations by inverting them. In *Proceedings of the IEEE conference on computer vision and pattern recognition*, pages 5188–5196, 2015.
- [38] Stylianos Moschoglou, Athanasios Papaioannou, Christos Sagonas, Jiankang Deng, Irene Kotsia, and Stefanos Zafeiriou. Agedb: the first manually collected, in-the-wild age database. In *proceedings of the IEEE conference on computer vision and pattern recognition workshops*, pages 51–59, 2017.
- [39] Mohammed Bany Muhammad and Mohammed Yeasin. Eigen-cam: Class activation map using principal components. In *2020 International Joint Conference on Neural Networks (IJCNN)*, pages 1–7. IEEE, 2020.
- [40] Timo Ojala, Matti Pietikäinen, and Topi Mäenpää. Gray scale and rotation invariant texture classification with local binary patterns. In *European Conference on Computer Vision*, pages 404–420. Springer, 2000.
- [41] Timo Ojala, Matti Pietikainen, and Topi Maenpaa. Multiresolution gray-scale and rotation invariant texture classification with local binary patterns. *IEEE Transactions on pattern analysis and machine intelligence*, 24(7):971–987, 2002.
- [42] Omkar M Parkhi, Andrea Vedaldi, and Andrew Zisserman. Deep face recognition. 2015.
- [43] MB Prime and AT DeWald. Practical residual stress measurement methods: The contour method, 2013.
- [44] Michael B Prime and Adrian T DeWald. The contour method. *Practical residual stress measurement methods*, pages 109–138, 2013.
- [45] Yong Qi, Huawei Lin, Yanping Li, and Jiashu Chen. Parameter-free attention in fmri decoding. *IEEE Access*, 9:48704–48712, 2021.
- [46] Yong Qi, Menzhe Qiu, Huawei Lin, Jiashu Chen, Yanping Li, and Hongguang Lei. Research on gender-related fingerprint features, extracting fingerprint features using autoencoder networks for gender classification. 2022.
- [47] Harish Guruprasad Ramaswamy et al. Ablation-cam: Visual explanations for deep convolutional network via gradient-free localization. In *Proceedings of the IEEE/CVF Winter Conference on Applications of Computer Vision*, pages 983–991, 2020.
- [48] Christos Sagonas, Epameinondas Antonakos, Georgios Tzimiropoulos, Stefanos Zafeiriou, and Maja Pantic. 300 faces in-the-wild challenge: Database and results. *Image and vision computing*, 47:3–18, 2016.
- [49] Christos Sagonas, Georgios Tzimiropoulos, Stefanos Zafeiriou, and Maja Pantic. A semi-automatic methodology for facial landmark annotation. In *Proceedings of the IEEE conference on computer vision and pattern recognition workshops*, pages 896–903, 2013.
- [50] Florian Schroff, Dmitry Kalenichenko, and James Philbin. Facenet: A unified embedding for face recognition and clustering. In *Proceedings of the IEEE conference on computer vision and pattern recognition*, pages 815–823, 2015.
- [51] Ramprasaath R Selvaraju, Michael Cogswell, Abhishek Das, Ramakrishna Vedantam, Devi Parikh, and Dhruv Batra. Grad-cam: Visual explanations from deep networks via gradient-based localization. In *Proceedings of the IEEE international conference on computer vision*, pages 618–626, 2017.
- [52] Soumyadip Sengupta, Jun-Cheng Chen, Carlos Castillo, Vishal M Patel, Rama Chellappa, and David W Jacobs. Frontal to profile face verification in the wild. In *2016 IEEE*

- winter conference on applications of computer vision (WACV), pages 1–9. IEEE, 2016.
- [53] Karen Simonyan, Andrea Vedaldi, and Andrew Zisserman. Deep inside convolutional networks: Visualising image classification models and saliency maps. In *In Workshop at International Conference on Learning Representations*. Citeseer, 2014.
- [54] Karen Simonyan and Andrew Zisserman. Very deep convolutional networks for large-scale image recognition. *arXiv preprint arXiv:1409.1556*, 2014.
- [55] Yi Sun, Xiaogang Wang, and Xiaoou Tang. Deep learning face representation from predicting 10,000 classes. In *Proceedings of the IEEE conference on computer vision and pattern recognition*, pages 1891–1898, 2014.
- [56] Yaniv Taigman, Ming Yang, Marc Aurelio Ranzato, and Lior Wolf. Deepface: Closing the gap to human-level performance in face verification. In *Proceedings of the IEEE conference on computer vision and pattern recognition*, pages 1701–1708, 2014.
- [57] Feng Wang, Xiang Xiang, Jian Cheng, and Alan Loddon Yuille. Normface: L2 hypersphere embedding for face verification. In *Proceedings of the 25th ACM international conference on Multimedia*, pages 1041–1049, 2017.
- [58] Hao Wang, Yitong Wang, Zheng Zhou, Xing Ji, Dihong Gong, Jingchao Zhou, Zhifeng Li, and Wei Liu. Cosface: Large margin cosine loss for deep face recognition. In *Proceedings of the IEEE conference on computer vision and pattern recognition*, pages 5265–5274, 2018.
- [59] Haofan Wang, Zifan Wang, Mengnan Du, Fan Yang, Zijian Zhang, Sirui Ding, Piotr Mardziel, and Xia Hu. Score-cam: Score-weighted visual explanations for convolutional neural networks. In *Proceedings of the IEEE/CVF conference on computer vision and pattern recognition workshops*, pages 24–25, 2020.
- [60] Yandong Wen, Kaipeng Zhang, Zhifeng Li, and Yu Qiao. A discriminative feature learning approach for deep face recognition. In *European conference on computer vision*, pages 499–515. Springer, 2016.
- [61] Jingtian Xia, Siyang Song, Yan Tang, and Linlin Shen. Analyzing facial temporal patterns for face anti-spoofing. In *Proceedings of the 2020 9th International Conference on Computing and Pattern Recognition*, pages 200–207, 2020.
- [62] Jia Xiang and Gengming Zhu. Joint face detection and facial expression recognition with mtcnn. In *2017 4th international conference on information science and control engineering (ICISCE)*, pages 424–427. IEEE, 2017.
- [63] Zhanjia Yang, Xiangping Zhu, Changyuan Jiang, Wenshuang Liu, and Linlin Shen. Ramface: Race adaptive margin based face recognition for racial bias mitigation. In *2021 IEEE International Joint Conference on Biometrics (IJCB)*, pages 1–8. IEEE, 2021.
- [64] Bangjie Yin, Luan Tran, Haoxiang Li, Xiaohui Shen, and Xiaoming Liu. Towards interpretable face recognition. In *Proceedings of the IEEE/CVF International Conference on Computer Vision*, pages 9348–9357, 2019.
- [65] Timothy Zee, Geeta Gali, and Ifeoma Nwogu. Enhancing human face recognition with an interpretable neural network. In *Proceedings of the IEEE/CVF International Conference on Computer Vision Workshops*, pages 0–0, 2019.
- [66] Matthew D Zeiler and Rob Fergus. Visualizing and understanding convolutional networks. In *European conference on computer vision*, pages 818–833. Springer, 2014.
- [67] Quanshi Zhang, Xin Wang, Ying Nian Wu, Huilin Zhou, and Song-Chun Zhu. Interpretable cnns for object classification. *IEEE transactions on pattern analysis and machine intelligence*, 43(10):3416–3431, 2020.
- [68] Quanshi Zhang, Ying Nian Wu, and Song-Chun Zhu. Interpretable convolutional neural networks. In *Proceedings of the IEEE Conference on Computer Vision and Pattern Recognition*, pages 8827–8836, 2018.
- [69] Quanshi Zhang and Song-Chun Zhu. Visual interpretability for deep learning: a survey. *arXiv preprint arXiv:1802.00614*, 2018.
- [70] Wentian Zhang, Haozhe Liu, Raghavendra Ramachandra, Feng Liu, Linlin Shen, and Christoph Busch. Face presentation attack detection using taskonomy feature. *arXiv preprint arXiv:2111.11046*, 2021.
- [71] Kai Zhao, Jingyi Xu, and Ming-Ming Cheng. Regularface: Deep face recognition via exclusive regularization. In *Proceedings of the IEEE/CVF Conference on Computer Vision and Pattern Recognition*, pages 1136–1144, 2019.
- [72] Tianyue Zheng, Weihong Deng, and Jiani Hu. Cross-age lfw: A database for studying cross-age face recognition in unconstrained environments. *arXiv preprint arXiv:1708.08197*, 2017.
- [73] Yutong Zheng, Dipan K Pal, and Marios Savvides. Ring loss: Convex feature normalization for face recognition. In *Proceedings of the IEEE conference on computer vision and pattern recognition*, pages 5089–5097, 2018.
- [74] Yaoyao Zhong and Weihong Deng. Deep difference analysis in similar-looking face recognition. In *2018 24th International Conference on Pattern Recognition (ICPR)*, pages 3353–3358. IEEE, 2018.
- [75] Bolei Zhou, David Bau, Aude Oliva, and Antonio Torralba. Interpreting deep visual representations via network dissection. *IEEE transactions on pattern analysis and machine intelligence*, 41(9):2131–2145, 2018.
- [76] Bolei Zhou, Aditya Khosla, Agata Lapedriza, Aude Oliva, and Antonio Torralba. Learning deep features for discriminative localization. In *Proceedings of the IEEE conference on computer vision and pattern recognition*, pages 2921–2929, 2016.
- [77] Xiangxin Zhu and Deva Ramanan. Face detection, pose estimation, and landmark localization in the wild. In *2012 IEEE conference on computer vision and pattern recognition*, pages 2879–2886. IEEE, 2012.